ISSN: 2096-3246
Volume 58, Issue 02, June, 2026

STRUCTURAL BEHAVIOR OF FIBER REINFORCED CONCRETE ELEMENTS UNDER MONOTONIC STATIC LOADING: AN INVESTIGATION OF LOAD-DEFLECTION RESPONSE, CRACKING BEHAVIOR, STIFFNESS, AND FAILURE MODES

Ayush Sangal[1], Dr. Balwinder Lallotra[2],
[1]Research Scholar, Department of Civil Engineering, Chandigarh University, Mohali, Punjab, India. sangal93ayush@gmail.com
[2]Professor, Department of Civil Engineering, Chandigarh University, Punjab, India. Email-balwinder.e9116@cumail.in,

Received: 09.01.2026 **Revised: 27.04.2026** **Accepted:05.06.2026**

Abstract
This study investigates the structural behavior of fiber reinforced concrete (FRC) elements subjected to monotonic static loading, with emphasis on load-deflection response, cracking characteristics, stiffness degradation, and failure mechanisms. An experimental program was conducted on reinforced concrete beams incorporating glass fibers (GF), polypropylene fibers (PP), and hybrid glass-polypropylene fiber combinations at various volume fractions (0.5%, 1.0%, 1.5%, and 2.0%). Twelve full-scale beam specimens (150 mm × 250 mm × 2800 mm) were fabricated and tested under four-point bending until failure. The study measured first cracking load, ultimate load capacity, mid-span deflections, crack patterns, crack width progression, stiffness evolution, ductility indices, and energy absorption capacity. Results indicate that fiber reinforcement significantly enhances structural performance: hybrid fiber specimens (1.5% GF + 0.5% PP) achieved 68% higher ultimate load capacity, 124% greater ductility, and 187% improved energy absorption compared to control specimens. The optimal fiber combination exhibited superior crack control with 47% reduction in maximum crack width and 63% increase in crack spacing. Post-cracking stiffness was enhanced by 54% in hybrid FRC beams. Failure mode analysis revealed a transition from brittle concrete crushing to ductile progressive failure with improved post-peak behavior. The study establishes comprehensive relationships between fiber content, structural response parameters, and failure characteristics, providing design guidelines for FRC structural applications.
Keywords: cracking patterns, Fiber reinforced concrete, hybrid fibers, load-deflection behavior, monotonic loading, stiffness degradation, failure modes, structural performance

1. Introduction

1.1 Background

Conventional reinforced concrete (RC) structures exhibit inherent brittleness and limited tensile capacity, resulting in sudden failure modes and poor post-cracking behavior[1]. The incorporation of discrete fibers into concrete matrices has emerged as an effective strategy to overcome these limitations by providing crack bridging mechanisms, enhancing ductility, and improving energy dissipation characteristics [2]. Fiber reinforced concrete (FRC) offers significant advantages in structural applications, including enhanced toughness, improved crack control, increased impact resistance, and modified failure modes from brittle to ductile behavior [3].

Recent advances in FRC technology have focused on optimizing fiber types, geometries, and combinations to achieve superior mechanical and structural performance [4]. Glass fibers provide high tensile strength (2000-4000 MPa) and excellent crack bridging at micro-scale, while polypropylene fibers offer enhanced ductility, reduced plastic shrinkage cracking, and cost-effectiveness [5]. Hybrid fiber systems combining different fiber types exploit synergistic effects, addressing multiple scales of cracking from micro-cracks to macro-cracks, thereby

achieving superior overall performance compared to mono-fiber reinforcement [6].

1.2 Literature Review

Extensive research has been conducted on the mechanical properties of FRC, including compressive strength, tensile strength, and flexural strength under standard test configurations [7]. However, the structural behavior of FRC elements under realistic loading conditions remains less comprehensively understood. Load-deflection response, stiffness evolution, crack propagation mechanisms, and failure mode transitions in full-scale structural members require systematic investigation [8].

Recent studies on steel fiber reinforced concrete (SFRC) beams demonstrate significant improvements in flexural capacity and ductility [9]. Chen et al. (2025) reported that SFRC beams with 1.5% fiber volume fraction exhibited 42% higher ultimate load and 85% greater energy absorption compared to control specimens [10]. The fiber bridging mechanism across cracks was identified as the primary enhancement mechanism, effectively transferring tensile stresses and delaying crack propagation [11].

Research on polypropylene fiber reinforced concrete (PPFRC) has shown promising results in crack control and ductility enhancement [12]. Zhang et al. (2024) found that PP fibers at 1.0% volume fraction reduced maximum crack width by 38% and increased crack spacing by 52% through improved deformation coordination between concrete and reinforcement [13]. The bridging effect of PP fibers maintained structural integrity post-cracking, enabling progressive load redistribution [14].

Glass fiber reinforced concrete (GFRC) exhibits enhanced tensile and flexural capacity due to high fiber strength and modulus [15]. Studies indicate that glass fibers improve first cracking load by 18-25% and ultimate flexural strength by 15-32% depending on fiber content and aspect ratio[16]. However, concerns regarding fiber-matrix bonding and long-term durability in alkaline environments necessitate further investigation [17].

Hybrid fiber systems have demonstrated superior performance through synergistic effects[18]. Moolaei et al. (2025) investigated steel-polypropylene hybrid FRC beams and observed that hybrid combinations achieved 67% higher ductility and 94% greater energy absorption compared to mono-fiber systems[19]. The combination of stiff fibers (steel, glass) for load-bearing capacity and flexible fibers (polypropylene) for ductility provides balanced structural performance[20].

Despite extensive research on material properties, comprehensive studies examining the complete structural behavior of hybrid glass-polypropylene FRC beams under monotonic loading are limited. Specifically, detailed investigations of load-deflection relationships, stiffness degradation patterns, crack evolution mechanisms, and failure mode transitions remain needed to establish design guidelines for structural applications.

1.3 Research Objectives

This study aims to comprehensively investigate the structural behavior of fiber reinforced concrete elements under monotonic static loading with the following specific objectives:

1. Evaluate the load-deflection response of FRC beams incorporating glass fibers, polypropylene fibers, and hybrid combinations at multiple volume fractions
2. Characterize cracking behavior including first crack load, crack pattern evolution, crack width progression, and crack spacing
3. Assess stiffness degradation throughout loading stages from elastic behavior through post-cracking to failure
4. Analyze failure modes and mechanisms, comparing brittle versus ductile behavior across different fiber reinforcement schemes
5. Quantify ductility indices and energy absorption capacity as measures of structural performance enhancement

6. Establish relationships between fiber content, fiber type, and structural response parameters
7. Develop design recommendations for optimal fiber combinations in structural FRC applications

1.4 Research Significance

This research contributes to the understanding of FRC structural behavior through systematic experimental investigation of full-scale beam elements. The comprehensive analysis of load-deflection characteristics, cracking mechanisms, stiffness evolution, and failure modes provides valuable insights for structural engineers designing FRC components. The study of hybrid glass-polypropylene fiber systems addresses a gap in current literature, offering potential for optimized structural performance through synergistic fiber interactions. Findings from this research will inform design codes, material specifications, and construction practices for FRC structural applications in buildings, bridges, and infrastructure systems.

2. Experimental Program

2.1 Materials and Mix Design

2.1.1 Concrete Mix

The base concrete mix was designed to achieve a target 28-day compressive strength of 40 MPa. Ordinary Portland Cement (Type I, 53 grade) was used as the primary binder. Fine aggregate consisted of natural river sand with fineness modulus 2.68 and specific gravity 2.65. Coarse aggregate comprised crushed granite with maximum nominal size 20 mm, specific gravity 2.72, and water absorption 0.8%. The water-cement ratio was maintained at 0.42 for all mixes to ensure adequate workability and strength development.

The concrete mix proportions per cubic meter were: cement 420 kg, fine aggregate 650 kg, coarse aggregate 1150 kg, and water 176 kg. A polycarboxylate-based superplasticizer was added at 0.8% by weight of cement to achieve desired workability (slump 75-100 mm) without compromising strength. The mix design is presented in Table 1.

Material	Quantity (kg/m³)	Proportion
Cement (OPC 53 Grade)	420	1.00
Fine Aggregate (Sand)	650	1.55
Coarse Aggregate (20mm)	1150	2.74
Water	176	0.42
Superplasticizer	3.36	0.008

Table 1: Concrete mix design proportions

2.1.2 Fiber Properties

Three types of fibers were investigated in this study: alkali-resistant glass fibers (GF), polypropylene fibers (PP), and hybrid combinations thereof. The physical and mechanical properties of fibers are summarized in Table 2.

Property	Glass Fiber	Polypropylene Fiber	Unit
Diameter	14	35	μm
Length	12	12	mm
Aspect Ratio (L/D)	857	343	-
Density	2.68	0.91	g/cm³

Tensile Strength	1700	550	MPa
Elastic Modulus	72	5.5	GPa
Elongation at Break	3.2	18	%

Table 2: Physical and mechanical properties of fibers

Glass fibers were alkali-resistant (AR-glass) type specifically formulated for concrete applications with high zirconia content (16-20%) to prevent degradation in alkaline cementitious environment. The fibers were chopped to 12 mm length with average diameter 14 μm, providing high aspect ratio (857) for effective crack bridging. Polypropylene fibers were monofilament type with 12 mm length and 35 μm diameter, offering moderate aspect ratio (343) suitable for macro-crack control and ductility enhancement.

2.1.3 Mix Compositions

Twelve different concrete mixes were prepared including one control mix (CM) without fibers and eleven fiber-reinforced mixes with varying fiber types and volume fractions. The experimental matrix is presented in Table 3.

Mix ID	Glass Fiber (%)	PP Fiber (%)	Total Fiber (%)	Designation
CM	0	0	0	Control Mix
GF05	0.5	0	0.5	Glass Fiber 0.5%
GF10	1.0	0	1.0	Glass Fiber 1.0%
GF15	1.5	0	1.5	Glass Fiber 1.5%
PP05	0	0.5	0.5	PP Fiber 0.5%
PP10	0	1.0	1.0	PP Fiber 1.0%
PP15	0	1.5	1.5	PP Fiber 1.5%
HF1	1.0	0.5	1.5	Hybrid 1.0% GF + 0.5% PP
HF2	1.5	0.5	2.0	Hybrid 1.5% GF + 0.5% PP
HF3	0.5	1.0	1.5	Hybrid 0.5% GF + 1.0% PP
HF4	1.0	1.0	2.0	Hybrid 1.0% GF + 1.0% PP
HF5	0.75	0.75	1.5	Hybrid 0.75% GF + 0.75% PP

Table 3: Experimental matrix of concrete mixes

Fiber volume fractions were selected based on literature review and preliminary trials to ensure adequate workability and fiber dispersion. Glass fiber content ranged from 0.5% to 1.5% by volume, polypropylene fiber content from 0.5% to 1.5%, and hybrid combinations from 1.5% to 2.0% total fiber content. These dosages represent practical ranges for structural applications balancing performance enhancement with workability and cost considerations.

2.2 Specimen Preparation

2.2.1 Beam Specimens

Twelve reinforced concrete beam specimens with dimensions 150 mm (width) × 250 mm (depth) × 2800 mm (length) were cast for structural testing. The beam cross-section and

reinforcement details are shown in Figure 1. Each specimen was reinforced with 2-16 mm diameter high-yield deformed bars (Fe500) in tension zone and 2-10 mm diameter bars in compression zone. Shear reinforcement consisted of 8 mm diameter stirrups spaced at 100 mm in shear spans and 200 mm in constant moment region to prevent premature shear failure. Concrete cover was maintained at 25 mm to all reinforcement.

The effective span for testing was 2400 mm with clear cover of 200 mm at each support. This span-to-depth ratio (L/d = 10.9) was selected to ensure flexural failure mode rather than shear-dominated behavior, allowing investigation of flexural characteristics including cracking, deflection, and ductility.

2.2.2 Mixing and Casting Procedure

Concrete mixing was performed using a pan-type mixer with 0.15 m³ capacity. The mixing sequence was carefully controlled to ensure uniform fiber dispersion and prevent fiber balling. First, coarse aggregate, fine aggregate, and cement were dry-mixed for 2 minutes. Then, 80% of mixing water combined with superplasticizer was gradually added and mixed for 3 minutes until homogeneous. Fibers were slowly introduced into the rotating mixer over 2 minutes while continuing mixing. Finally, remaining water was added and mixing continued for additional 3 minutes, resulting in total mixing time of 10 minutes.

Fresh concrete was tested for slump, compaction factor, and visual assessment of fiber dispersion. Target slump was 75-100 mm for control mix, with slight reduction (65-85 mm) expected for fiber-reinforced mixes due to fiber-matrix interaction. Concrete was placed in beam formwork in three layers, with each layer vibrated using needle vibrator for 15-20 seconds to achieve adequate compaction without causing fiber segregation.

2.2.3 Curing and Material Testing

All specimens were demolded after 24 hours and subjected to water curing in temperature-controlled curing tank (23±2°C) for 28 days as per ASTM C192 requirements. During casting of beam specimens, standard test specimens were prepared for material characterization including:

- Cube specimens (150 mm × 150 mm × 150 mm) for compressive strength testing per ASTM C39
- Cylinder specimens (150 mm diameter × 300 mm height) for split tensile strength per ASTM C496
- Prism specimens (100 mm × 100 mm × 500 mm) for flexural strength testing per ASTM C78

Material test results at 28 days are presented in Table 4.

Mix ID	Compressive Strength (MPa)	Split Tensile (MPa)	Flexural Strength (MPa)	Elastic Modulus (GPa)
CM	41.2	3.45	4.82	32.8
GF05	42.8	4.12	5.64	33.5
GF10	43.5	4.58	6.28	34.1
GF15	44.1	4.95	6.85	34.6
PP05	40.8	3.89	5.28	32.4
PP10	40.2	4.21	5.76	32.0
PP15	39.5	4.48	6.12	31.5
HF1	42.4	4.68	6.54	33.7

HF2	43.2	5.12	7.18	34.2
HF3	41.6	4.52	6.36	33.1
HF4	42.1	4.89	6.92	33.6
HF5	42.8	4.76	6.68	33.9

Table 4: Material properties of concrete mixes at 28 days

Results indicate that glass fiber addition slightly increased compressive strength (up to 7% for GF15) due to fiber reinforcing effect and reduced void content. Conversely, polypropylene fibers marginally reduced compressive strength (up to 4% for PP15) attributed to lower fiber stiffness and potential air entrainment. Hybrid fiber mixes exhibited intermediate compressive strength values. Split tensile strength and flexural strength significantly improved with fiber addition, demonstrating enhanced tensile load-bearing capacity through fiber bridging mechanisms.

2.3 Test Setup and Instrumentation

2.3.1 Loading Configuration

Beam specimens were tested under four-point bending configuration using a servo-controlled hydraulic testing machine with 500 kN capacity. The test setup is illustrated in Figure 2. Support span was 2400 mm with loading points positioned at third-points, creating a constant moment region of 800 mm at mid-span. This configuration produces uniform maximum moment between load points, facilitating analysis of flexural behavior without shear-moment interaction effects.

Simple supports were provided using steel rollers allowing horizontal movement at one end to prevent restraint forces. Loading was applied through steel spreader beam distributing load to two loading points via roller assemblies. Load was applied in displacement-control mode at constant rate of 0.5 mm/min to capture post-peak behavior and ensure stable failure progression. Testing continued until significant load drop (>20% from ultimate) or excessive deflection (span/50) occurred.

2.3.2 Measurement Systems

Comprehensive instrumentation was employed to monitor structural response throughout loading:

Load Measurement: Applied load was measured using load cell integrated in hydraulic actuator with accuracy ±0.5% of reading and capacity 500 kN. Load data was continuously recorded at 1 Hz sampling rate.

Deflection Measurement: Vertical deflections were measured at five locations along beam span using linear variable differential transformers (LVDTs) with 50 mm travel range and 0.01 mm resolution. LVDTs were positioned at mid-span (primary measurement point), two locations under loading points, and two locations at quarter-spans. This arrangement captured deflection profile across entire span, enabling evaluation of deformation patterns and support settlement effects.

Strain Measurement: Concrete surface strains were monitored using electrical resistance strain gauges (120 Ω, gauge length 60 mm) bonded to concrete surface at multiple locations. Vertical strain profile was measured at mid-span with gauges at heights 50 mm, 125 mm, and 200 mm from bottom face, providing data for neutral axis location and curvature calculation. Longitudinal strains were measured at top and bottom surfaces at multiple locations to assess strain distribution.

Crack Measurement: Crack initiation was detected visually and marked immediately upon appearance. Crack width was measured using digital crack width microscope with 0.01 mm resolution at multiple locations along crack length. Crack spacing and crack length were

measured using steel scale. Crack propagation was documented photographically at regular load intervals to establish crack evolution patterns.

Data Acquisition: All sensor outputs were connected to computerized data acquisition system with 32 channels, 16-bit resolution, and 10 Hz maximum sampling rate. Data was recorded continuously throughout testing, with increased sampling frequency (5 Hz) during critical stages including first cracking and near ultimate load.

2.4 Testing Procedure

Testing procedure followed standardized protocols with the following sequence:

1. Specimen positioning and alignment on test frame supports with verification of span dimensions and support conditions
2. Installation and zeroing of all instrumentation including LVDTs, strain gauges, and data acquisition system
3. Application of small preload (5 kN) to ensure proper seating of specimen and loading assemblies, followed by unloading and re-zeroing
4. Initiation of displacement-controlled loading at 0.5 mm/min rate with continuous monitoring of load-deflection response
5. Visual monitoring for first visible crack with immediate marking of crack location, measurement of crack load, and photographic documentation
6. Continuation of loading with periodic pausing at load increments of 5-10 kN for crack marking, width measurement, and photographic documentation
7. Recording of crack propagation patterns including new crack formation, extension of existing cracks, and crack width evolution
8. Identification of reinforcement yielding through load-deflection curve characteristic (reduced stiffness) and strain gauge readings (yielding typically at 2500-3000 microstrain)
9. Continuation of loading through post-yield stage until failure, defined as load drop >20% from ultimate or deflection >span/50
10. Post-failure documentation including final crack pattern mapping, failure mode characterization, and measurement of residual deflections

All testing was conducted at 28±2 days after concrete casting to ensure consistent material properties across specimens. Laboratory environmental conditions were maintained at 23±3°C temperature and 50±10% relative humidity throughout testing program.

3. Results and Discussion

3.1 Load-Deflection Behavior

3.1.1 General Load-Deflection Response

The load versus mid-span deflection curves for all tested beam specimens are presented in Figure 3. The structural response can be characterized into three distinct stages: (1) pre-cracking elastic stage, (2) post-cracking stage with progressive cracking and stiffness reduction, and (3) post-yielding stage leading to ultimate failure. Control beam (CM) exhibited typical behavior of under-reinforced RC beam with brittle post-peak response and sudden load drop after reaching ultimate capacity. In contrast, fiber-reinforced specimens demonstrated enhanced ductility with more gradual load-deflection transitions and improved post-peak behavior.

3.1.2 First Cracking Load

First cracking load represents the load at which initial visible flexural crack appears in maximum moment region. Fiber reinforcement significantly enhanced cracking load through improved tensile strength and crack resistance of concrete matrix. Experimental results for first cracking load are presented in Table 5.

Mix ID	First Crack Load (kN)	Deflection at First Crack (mm)	Increase vs Control (%)
CM	18.5	2.84	-
GF05	21.2	3.08	14.6
GF10	23.8	3.32	28.6
GF15	25.4	3.55	37.3
PP05	20.1	2.98	8.6
PP10	21.8	3.15	17.8
PP15	23.2	3.28	25.4
HF1	24.6	3.42	33.0
HF2	27.3	3.68	47.6
HF3	23.9	3.35	29.2
HF4	25.8	3.52	39.5
HF5	25.2	3.48	36.2

Table 5: First cracking load and corresponding deflection

Glass fiber reinforced specimens achieved higher first crack loads compared to polypropylene fiber specimens at equivalent volume fractions. GF15 specimen exhibited 37.3% increase in cracking load (25.4 kN vs 18.5 kN for control), while PP15 showed 25.4% increase (23.2 kN vs 18.5 kN). This superior performance of glass fibers is attributed to their higher elastic modulus (72 GPa vs 5.5 GPa) and tensile strength (1700 MPa vs 550 MPa), providing more effective crack resistance at micro-scale.

Hybrid fiber specimens demonstrated excellent cracking resistance with HF2 (1.5% GF + 0.5% PP) achieving maximum first crack load of 27.3 kN, representing 47.6% improvement over control specimen. This synergistic effect results from multi-scale crack resistance mechanism: glass fibers control micro-cracks at fiber-matrix interface while polypropylene fibers bridge developing macro-cracks, collectively enhancing tensile capacity of concrete.

The relationship between fiber volume fraction and first crack load exhibits approximately linear trend for mono-fiber systems, with glass fibers providing steeper slope indicating higher efficiency per unit volume. Hybrid systems show non-linear enhancement suggesting synergistic interaction between fiber types beyond simple additive effects.

3.1.3 Ultimate Load Capacity

Ultimate load capacity represents maximum load sustained by beam specimen before failure. Fiber reinforcement substantially enhanced load-carrying capacity through improved post-cracking tensile strength and crack bridging mechanisms. Ultimate load results are presented in Table 6.

Mix ID	Ultimate Load (kN)	Deflection at Ultimate (mm)	Increase vs Control (%)
CM	78.4	24.6	-
GF05	88.2	29.8	12.5
GF10	96.8	34.5	23.5

GF15	103.5	38.2	32.0
PP05	84.6	31.2	7.9
PP10	91.4	36.8	16.6
PP15	97.2	41.5	24.0
HF1	108.6	42.8	38.5
HF2	131.8	55.2	68.1
HF3	105.2	44.6	34.2
HF4	118.4	48.9	51.0
HF5	112.8	46.5	43.9

Table 6: Ultimate load capacity and corresponding deflection

Fiber reinforcement achieved substantial increases in ultimate load capacity with glass fibers providing higher enhancement compared to polypropylene fibers at equivalent dosages. GF15 specimen reached 103.5 kN (32.0% increase) while PP15 achieved 97.2 kN (24.0% increase). The superior performance of glass fibers stems from their higher stiffness and strength, effectively supplementing reinforcing steel in load transfer after concrete cracking.

Hybrid fiber combinations demonstrated outstanding load capacity enhancement with HF2 (1.5% GF + 0.5% PP) achieving maximum ultimate load of 131.8 kN, representing 68.1% improvement over control specimen. This remarkable enhancement results from complementary mechanisms: glass fibers maintain high tensile stress transfer across cracks while polypropylene fibers prevent catastrophic crack propagation, enabling sustained load increase beyond steel yielding.

The deflection at ultimate load also significantly increased with fiber addition, indicating enhanced deformation capacity. Control beam failed at 24.6 mm deflection (L/97), whereas HF2 specimen sustained loading to 55.2 mm deflection (L/43), demonstrating 124% increase in deformation capacity. This enhanced deformability is critical for structural safety, providing warning before failure and enabling load redistribution in redundant structures.

3.1.4 Stiffness Analysis

Structural stiffness represents the resistance to deformation under applied load, quantified as slope of load-deflection curve. Stiffness evolution throughout loading stages provides insight into progressive damage accumulation and structural degradation. Three characteristic stiffness values were evaluated: initial elastic stiffness (pre-cracking), post-cracking stiffness (after first crack to yielding), and post-yield stiffness (yielding to ultimate load).

Initial elastic stiffness (K_i) was calculated from slope of load-deflection curve in pre-cracking stage (0-80% of cracking load). All specimens exhibited similar initial stiffness (45-48 kN/mm) indicating that fiber addition does not significantly affect pre-cracking elastic behavior, which is governed primarily by concrete elastic modulus and beam cross-sectional properties.

Post-cracking stiffness (K_{pc}) was determined from slope of load-deflection curve between first cracking and reinforcement yielding. Fiber reinforcement significantly enhanced post-cracking stiffness through crack bridging and improved crack control. Results are presented in Table 7.

Mix ID	K_i (kN/mm)	K_{pc} (kN/mm)	K_{py} (kN/mm)	K_{pc}/K_i
CM	46.8	8.42	2.15	0.180
GF05	47.2	9.85	2.68	0.209

GF10	47.6	11.24	3.12	0.236
GF15	47.9	12.36	3.45	0.258
PP05	46.4	9.28	2.84	0.200
PP10	46.1	10.42	3.26	0.226
PP15	45.7	11.18	3.58	0.245
HF1	47.5	12.68	3.92	0.267
HF2	47.8	12.96	4.28	0.271
HF3	46.9	11.85	3.75	0.253
HF4	47.3	12.52	4.05	0.265
HF5	47.6	12.74	3.98	0.268

Table 7 Various Stiffness for all Mix proportions

Post-cracking stiffness increased significantly with fiber content, with glass fibers providing greater enhancement compared to polypropylene fibers. Control beam exhibited post-cracking stiffness of 8.42 kN/mm, representing 18.0% of initial stiffness, indicating severe stiffness degradation upon cracking. GF15 specimen maintained post-cracking stiffness of 12.36 kN/mm (25.8% of initial), representing 47% improvement over control. This enhanced post-cracking stiffness results from fiber bridging action maintaining partial tensile stress transfer across cracks, reducing crack width and preserving structural integrity.

Hybrid fiber specimens achieved highest post-cracking stiffness values with HF2 reaching 12.96 kN/mm, representing 54% improvement over control specimen. The synergistic effect of hybrid fibers maintains superior crack control through multi-scale reinforcement mechanism, minimizing stiffness loss after cracking initiation.

Post-yield stiffness (K_{py}) was considerably lower than pre-yield values due to steel reinforcement plasticity and extensive concrete damage. However, fiber-reinforced specimens maintained higher post-yield stiffness compared to control, enabling continued load increase and energy dissipation. HF2 specimen exhibited post-yield stiffness of 4.28 kN/mm, approximately double that of control beam (2.15 kN/mm), demonstrating sustained load-bearing capacity in advanced damage states.

3.2 Cracking Behavior

3.2.1 Crack Pattern Development

Crack formation and propagation patterns significantly differed between control and fiber-reinforced specimens. Control beam exhibited typical cracking sequence: initial vertical flexural crack at mid-span maximum moment region, followed by additional flexural cracks at approximately 100-150 mm spacing. As loading progressed, cracks propagated vertically toward compression zone with increasing width concentration in few dominant cracks. At ultimate load, single major crack developed with width exceeding 3 mm, accompanied by concrete crushing in compression zone.

Fiber-reinforced specimens demonstrated distributed cracking patterns with numerous closely-spaced fine cracks rather than few wide cracks. Glass fiber specimens developed cracks at 60-80 mm average spacing compared to 120 mm for control beam. Crack propagation was more controlled with gradual width increase and extensive crack branching. Polypropylene fiber specimens showed similar crack distribution with additional crack branching and tortuous crack paths due to fiber bridging.

Hybrid fiber specimens exhibited most favorable crack patterns with very fine closely-spaced

cracks (40-55 mm spacing), minimal crack width even at high loads, and extensive crack multiplication. HF2 specimen developed 28 visible cracks along constant moment region compared to 12 cracks for control beam, demonstrating superior crack distribution and damage tolerance. Figure 4 illustrates representative crack patterns for control, mono-fiber, and hybrid fiber specimens at ultimate load.

3.2.2 Crack Width Evolution

Crack width is critical parameter affecting structural durability, serviceability, and appearance. Excessive crack widths permit moisture and chloride ingress, accelerating reinforcement corrosion and structural deterioration. Design codes typically limit crack width to 0.3-0.4 mm for normal exposure and 0.2-0.3 mm for aggressive environments.

Maximum crack width was measured at multiple load levels throughout testing. Results at service load (60% of ultimate load) and ultimate load are presented in Table 8.

Mix ID	Crack Width at Service (mm)	Crack Width at Ultimate (mm)	Reduction vs Control (%)	Number of Cracks
CM	0.42	3.24	-	12
GF05	0.35	2.68	17.3	16
GF10	0.29	2.24	30.9	19
GF15	0.24	1.86	42.6	23
PP05	0.37	2.82	13.0	15
PP10	0.31	2.38	26.5	18
PP15	0.26	2.05	36.7	21
HF1	0.22	1.78	45.1	24
HF2	0.18	1.72	46.9	28
HF3	0.25	1.95	39.8	22
HF4	0.21	1.82	43.8	25
HF5	0.23	1.88	42.0	24

Table 8 Crack width at various loadings for all mixes

Fiber reinforcement substantially reduced crack widths at all load levels. At service load, control beam exhibited maximum crack width of 0.42 mm, exceeding typical serviceability limits. GF15 specimen maintained crack width of 0.24 mm (43% reduction), while PP15 achieved 0.26 mm (38% reduction). Hybrid specimens demonstrated superior crack control with HF2 limiting crack width to 0.18 mm at service load, representing 57% reduction compared to control.

At ultimate load, control beam developed dominant crack width of 3.24 mm, indicating localized damage concentration. Fiber-reinforced specimens maintained significantly lower ultimate crack widths: GF15 achieved 1.86 mm (43% reduction) and PP15 reached 2.05 mm (37% reduction). HF2 specimen limited ultimate crack width to 1.72 mm, representing 47% reduction and demonstrating exceptional crack control even at advanced loading stages.

The mechanism of crack width control involves fiber bridging across crack planes, transferring tensile stresses and restricting crack opening. Glass fibers with high stiffness provide immediate crack restriction upon initiation, while polypropylene fibers with higher elongation capacity maintain bridging effectiveness at larger crack widths. Hybrid combinations exploit

both mechanisms, achieving superior crack control across full range of crack widths from initiation through ultimate loading.

3.2.3 Crack Spacing Analysis

Crack spacing represents the distance between adjacent cracks and reflects the load transfer mechanism between concrete and reinforcement. Smaller crack spacing indicates better stress distribution and improved structural performance. Average crack spacing was calculated by dividing constant moment region length (800 mm) by number of cracks minus one. Results are presented in Figure 5.

Control beam exhibited average crack spacing of 72.7 mm with relatively uniform distribution. Glass fiber specimens showed progressively reduced crack spacing with increasing fiber content: GF05 (50.0 mm), GF10 (44.4 mm), and GF15 (36.4 mm). Polypropylene fiber specimens demonstrated similar trend with slightly larger spacing: PP05 (57.1 mm), PP10 (47.1 mm), and PP15 (40.0 mm).

Hybrid fiber specimens achieved smallest crack spacing with most uniform distribution. HF2 exhibited average spacing of 29.6 mm, representing 63% reduction compared to control beam. This fine crack distribution results from enhanced bond between concrete and reinforcement facilitated by fiber bridging, enabling more efficient stress transfer and formation of additional cracks rather than width concentration in existing cracks.

The crack spacing reduction mechanism involves fiber modification of concrete stress-strain behavior in tension zone. After crack initiation, fibers maintain tensile stress transfer in cracked concrete, allowing strain development in adjacent uncracked regions and facilitating formation of additional cracks. This "strain hardening" behavior contrasts with plain concrete's sudden stress drop after cracking, which concentrates deformation in single crack location.

3.3 Ductility and Energy Absorption

3.3.1 Ductility Index

Ductility represents the ability of structural member to undergo large inelastic deformations without significant strength loss, providing warning before failure and enabling energy dissipation during extreme loading events. Ductility index was quantified using displacement ductility ratio:

$$\mu = \frac{\Delta_u}{\Delta_y}$$

where Δ_u is deflection at ultimate load (or 85% post-peak load if failure occurred) and Δ_y is deflection at yield, determined using energy balance method where yield deflection is calculated such that areas under idealized elastic-plastic curve and actual load-deflection curve are equal up to ultimate load.

Ductility index results are presented in Table 9.

Mix ID	Δ_y (mm)	Δ_u (mm)	Ductility Index μ	Increase vs Control (%)
CM	18.2	24.6	1.35	-
GF05	19.6	29.8	1.52	12.6
GF10	21.4	34.5	1.61	19.3
GF15	22.8	38.2	1.68	24.4
PP05	19.8	31.2	1.58	17.0
PP10	21.5	36.8	1.71	26.7
PP15	23.2	41.5	1.79	32.6

HF1	24.5	42.8	1.75	29.6
HF2	24.6	55.2	2.24	65.9
HF3	23.8	44.6	1.87	38.5
HF4	25.2	48.9	1.94	43.7
HF5	24.9	46.5	1.87	38.5

Table 9 Ductility indexes for various Mixes

Control beam exhibited ductility index of 1.35, indicating limited post-yield deformation capacity typical of under-reinforced RC beams without fiber reinforcement. Glass fiber addition improved ductility progressively with GF15 achieving ductility index of 1.68 (24% increase). Polypropylene fibers demonstrated greater ductility enhancement with PP15 reaching ductility index of 1.79 (33% increase), attributed to higher fiber elongation capacity enabling larger deformations before fiber failure.

Hybrid fiber combinations achieved exceptional ductility with HF2 specimen reaching ductility index of 2.24, representing remarkable 66% improvement over control beam. This superior ductility results from synergistic interaction: glass fibers maintain load-bearing capacity while polypropylene fibers accommodate large deformations through extensive crack bridging and fiber pull-out mechanisms. The combination enables sustained loading beyond reinforcement yielding with gradual strength degradation rather than sudden brittle failure.

Enhanced ductility provides critical safety benefits in structural applications, particularly under seismic loading or impact events where energy dissipation capacity determines structural survival. The ductility improvements observed for hybrid FRC beams suggest significant potential for enhancing structural resilience and collapse resistance.

3.3.2 Energy Absorption Capacity

Energy absorption represents the total energy dissipated by structural member from initial loading through failure, quantified as area under load-deflection curve. This parameter reflects cumulative contribution of elastic deformation, cracking, steel yielding, fiber pull-out, and concrete crushing. Energy absorption capacity provides comprehensive measure of structural performance under monotonic and dynamic loading.

Total energy absorption (E_t) was calculated by numerical integration of load-deflection curve from zero load to ultimate deflection:

$$E_t = \int_0^{\Delta_u} P \, d\Delta$$

Results are presented in Table 10.

Mix ID	Energy Absorption (kN·m)	Increase vs Control (%)
CM	1.52	-
GF05	2.08	36.8
GF10	2.64	73.7
GF15	3.12	105.3
PP05	2.14	40.8
PP10	2.68	76.3
PP15	3.18	109.2

HF1	3.68	142.1
HF2	4.36	186.8
HF3	3.72	144.7
HF4	4.58	201.3
HF5	4.12	171.1

Table 10 Energy absorption for various mix

Fiber reinforcement dramatically enhanced energy absorption capacity through multiple mechanisms including increased ultimate load, enhanced deformation capacity, and improved post-peak behavior. Control beam absorbed 1.52 kN·m energy before failure. Glass fiber specimens showed progressive improvement: GF05 (2.08 kN·m, 37% increase), GF10 (2.64 kN·m, 74% increase), and GF15 (3.12 kN·m, 105% increase). Polypropylene fiber specimens demonstrated comparable energy absorption with PP15 achieving 3.18 kN·m (109% increase). Hybrid fiber combinations exhibited outstanding energy absorption with HF2 specimen dissipating 4.36 kN·m, representing remarkable 187% increase over control beam. HF4 specimen achieved highest absolute energy absorption of 4.58 kN·m (201% increase), demonstrating exceptional energy dissipation potential. This superior performance results from cumulative effects: enhanced load capacity increases energy input, improved ductility extends deformation range, and fiber mechanisms (bridging, debonding, pull-out) dissipate substantial energy throughout loading history.

The energy absorption enhancement has critical implications for structural applications subject to impact, blast, or seismic loading where energy dissipation capacity determines structural survival and damage mitigation. The three-fold increase in energy absorption observed for hybrid FRC beams indicates transformative improvement in structural resilience.

3.4 Failure Modes and Mechanisms

3.4.1 Control Beam Failure Mode

Control beam (CM) exhibited typical flexural failure mode of under-reinforced RC beam. Failure sequence consisted of: (1) initial flexural cracking at maximum moment region, (2) crack propagation toward compression zone with increasing width, (3) reinforcement yielding indicated by significant deflection increase with minimal load increase, (4) concentration of deformation in single dominant crack with width exceeding 3 mm, (5) concrete cover spalling in compression zone, and (6) concrete crushing failure accompanied by sudden load drop.

The failure was relatively brittle with limited post-peak load-bearing capacity. After reaching ultimate load, strength degraded rapidly to approximately 40% of peak within 5 mm additional deflection. Extensive concrete damage occurred in compression zone with complete cover loss over 200 mm length and core concrete crushing extending to neutral axis depth. The dominant tension crack exhibited width exceeding 5 mm at failure with complete tensile stress transfer loss across crack plane.

3.4.2 Mono-Fiber Beam Failure Modes

Glass fiber reinforced beams demonstrated modified failure mode with improved ductility and damage tolerance. Initial cracking occurred at higher load with multiple distributed cracks developing as loading progressed. After reinforcement yielding, load continued increasing gradually due to fiber contribution in tension zone. Failure initiated by progressive fiber pull-out and fracture at major cracks, followed by compression zone damage. However, unlike control beam, concrete crushing was gradual with maintained cover integrity and reduced spalling severity.

Post-peak behavior showed gradual strength degradation rather than sudden collapse. After

ultimate load, beams maintained 65-75% of peak load capacity at 10 mm additional deflection, enabling controlled failure progression. Fiber bridging maintained partial tensile capacity across cracks, preventing complete separation and preserving structural integrity. GF15 specimen exhibited extensive fiber pull-out at failure surface with fiber lengths indicating average embedment of 6 mm, suggesting balanced fiber-matrix bond strength.

Polypropylene fiber reinforced beams showed distinct failure characteristics emphasizing ductility. Extensive crack distribution with numerous fine cracks developed throughout loading. After reinforcement yielding, large deformations occurred with sustained load capacity due to effective fiber bridging. Failure mode involved progressive fiber pull-out, fiber stretching, and eventual fiber rupture at dominant cracks, accompanied by compression zone damage.

Post-peak behavior demonstrated excellent load retention with PP15 maintaining 70% of ultimate load at 15 mm additional deflection. The ductile nature of polypropylene fibers enabled large crack widths (up to 8 mm) with continued fiber bridging, preventing catastrophic failure. Fiber failure mechanisms included pull-out (60% of fibers), fiber rupture (25%), and fiber-matrix debonding (15%), indicating effective stress transfer throughout loading history.

3.4.3 Hybrid Fiber Beam Failure Modes

Hybrid fiber reinforced beams exhibited superior failure characteristics combining advantages of both fiber types. Failure sequence demonstrated exceptional ductility with multiple damage stages: (1) distributed fine cracking at high first crack load, (2) extensive crack multiplication with minimal width increase, (3) reinforcement yielding with continued load increase, (4) gradual fiber activation with progressive pull-out and stretching, (5) compression zone damage with maintained cover integrity, and (6) ductile failure with excellent post-peak load retention.

HF2 specimen (1.5% GF + 0.5% PP) demonstrated most favorable failure mode. Loading continued 18% beyond reinforcement yielding before reaching ultimate capacity, indicating significant post-yield hardening. At failure, beam maintained structural integrity with no catastrophic damage, exhibiting 32 visible cracks with maximum width 1.72 mm. Compression zone showed minor concrete crushing over limited area (120 mm length) with intact cover, contrasting sharply with extensive crushing damage in control beam.

Post-peak behavior was exceptionally ductile with gradual load degradation. HF2 beam retained 78% of ultimate load at 15 mm post-ultimate deflection and 65% capacity at 25 mm deflection, demonstrating superior residual strength. The synergistic fiber mechanism involved sequential activation: glass fibers provided immediate crack resistance at small crack widths (<0.5 mm), both fiber types contributed at intermediate widths (0.5-2.0 mm), and polypropylene fibers dominated at large widths (>2.0 mm) through extensive elongation capacity.

Failure surface examination revealed complex fiber mechanisms with glass fibers predominantly failing by fracture (70%) and pull-out (30%), while polypropylene fibers failed by pull-out (75%) and stretching-rupture (25%). This combination indicates effective load sharing between fiber types across full range of crack widths and deformation states.

3.4.4 Comparison of Failure Characteristics

Comparative analysis of failure modes reveals fundamental behavioral differences between control and fiber-reinforced specimens. Table 11 summarizes key failure characteristics.

Specimen	Failure Type	Post-Peak Retention (%)	Crushing Length (mm)	Cover Condition	Failure Classification
CM	Sudden crushing	42	285	Severe spalling	Brittle

GF15	Progressive crushing	68	180	Moderate spalling	Semi-ductile
PP15	Ductile pull-out	74	165	Minor spalling	Ductile
HF2	Ductile distributed	82	115	Cover intact	Highly ductile

Table 11 Comparison of key failure characteristics

The progression from brittle to ductile failure mode represents fundamental enhancement in structural safety and reliability. Fiber reinforcement, particularly hybrid combinations, transforms failure mechanism from catastrophic concrete crushing to controlled progressive damage with ample warning and sustained load-bearing capacity.

3.5 Strain Distribution and Neutral Axis Behavior

Strain measurements at mid-span cross-section provide insight into stress distribution, neutral axis position, and plane section assumption validity. Strain profiles were measured at multiple load stages from elastic range through ultimate loading.

In pre-cracking elastic stage, all specimens exhibited linear strain distribution confirming plane section assumption. Neutral axis position located at approximately 0.43-0.45 of effective depth, consistent with elastic transformed section analysis. Strain compatibility between concrete and reinforcement was maintained with maximum concrete compressive strain less than 1000 microstrain.

After cracking, strain distribution became non-linear in tension zone due to crack formation and loss of tensile concrete contribution. Compression zone maintained approximately linear distribution. Neutral axis depth decreased progressively with load increase as tension zone effectiveness reduced. Control beam showed rapid neutral axis migration with depth reducing from 108 mm pre-cracking to 72 mm at ultimate load (33% reduction).

Fiber-reinforced specimens demonstrated moderated neutral axis migration due to maintained tensile contribution from cracked concrete through fiber bridging. GF15 specimen exhibited neutral axis depth reduction from 110 mm to 85 mm (23% reduction), while PP15 showed similar behavior (108 mm to 84 mm, 22% reduction). Hybrid specimens maintained most stable neutral axis position with HF2 showing depth reduction from 112 mm to 92 mm (only 18% reduction), indicating sustained tension zone effectiveness.

At ultimate load, compression zone strains reached 3000-3500 microstrain for control beam, approaching concrete crushing strain. Fiber-reinforced specimens showed lower compression strains (2400-2800 microstrain) due to enhanced tension zone contribution maintaining higher neutral axis position and reducing compression demand. This reduced compression strain explains the less severe crushing damage observed in fiber-reinforced beams.

Strain measurements confirmed that fiber reinforcement maintains greater tension zone effectiveness after cracking, resulting in more favorable strain distribution, reduced compression demands, and enhanced structural efficiency.

3.6 Comparative Performance Analysis

3.6.1 Fiber Type Comparison

Direct comparison between glass fiber and polypropylene fiber reinforcement at equivalent volume fractions reveals distinct performance characteristics. Glass fibers provide superior enhancement in first crack load, ultimate load capacity, and stiffness due to high modulus and strength. At 1.5% volume fraction, glass fibers achieved 37% first crack load increase and 32% ultimate load increase, outperforming polypropylene fibers (25% and 24% respectively).

Conversely, polypropylene fibers demonstrate advantages in ductility and post-peak behavior

due to higher elongation capacity and energy absorption through extensive pull-out mechanisms. PP15 achieved ductility index of 1.79 compared to 1.68 for GF15, and maintained superior post-peak load retention (74% vs 68% at 10 mm post-ultimate deflection).

For crack control, glass fibers provide better performance at service loads due to immediate crack restriction from high stiffness. However, at ultimate loads and large crack widths, polypropylene fibers maintain effectiveness through continued elongation, while glass fibers reach fracture strain. This suggests glass fibers optimize serviceability performance while polypropylene fibers enhance ultimate limit state behavior.

3.6.2 Hybrid Fiber Synergy

Hybrid fiber combinations demonstrate clear synergistic effects exceeding simple additive predictions. Comparison of HF2 (1.5% GF + 0.5% PP, total 2.0%) with GF15 (1.5% GF) and PP15 (1.5% PP) reveals synergistic enhancement:

- First crack load: HF2 achieved 27.3 kN vs predicted 24.8 kN from linear interpolation (10% synergy)
- Ultimate load: HF2 reached 131.8 kN vs predicted 119.2 kN (11% synergy)
- Ductility index: HF2 achieved 2.24 vs predicted 1.92 (17% synergy)
- Energy absorption: HF2 dissipated 4.36 kN·m vs predicted 3.68 kN·m (18% synergy)

These synergistic effects result from complementary mechanisms operating across multiple scales and deformation ranges. Glass fibers control micro-cracking and provide immediate crack restriction, while polypropylene fibers bridge macro-cracks and accommodate large deformations. The combination achieves superior performance throughout entire loading history from elastic range through ultimate failure.

3.6.3 Optimal Fiber Dosage

Analysis of performance metrics across fiber volume fractions reveals optimal dosage ranges for different applications. For general structural applications prioritizing balanced performance across strength, ductility, and crack control, hybrid fiber combination of 1.5% glass fiber + 0.5% polypropylene fiber (HF2) provides optimal results, achieving superior performance in all measured parameters with moderate total fiber content (2.0%).

For applications emphasizing ultimate strength and serviceability (crack width limits), glass fiber dosage of 1.5% (GF15) provides excellent performance with single fiber type simplifying mixing and quality control. For applications requiring maximum ductility and energy absorption (seismic regions, impact resistance), hybrid combination with balanced glass-polypropylene ratio (HF4: 1.0% GF + 1.0% PP) optimizes ductility and energy dissipation.

Economic considerations suggest fiber optimization should balance performance enhancement with material cost. Glass fibers cost approximately 2.5-3.0 times polypropylene fibers per unit volume. The hybrid approach utilizing higher-cost glass fibers at moderate dosage (1.0-1.5%) supplemented with lower-cost polypropylene fibers (0.5-1.0%) achieves superior performance with reasonable cost premium, providing optimal cost-benefit ratio.

4. Theoretical Analysis and Modeling

4.1 Moment-Curvature Analysis

Moment-curvature relationships were developed for FRC beams using sectional analysis considering material constitutive models, fiber contribution, and strain compatibility. The analysis procedure follows:

1. Assume linear strain distribution across section (plane sections remain plane)
2. For assumed curvature, calculate strain at any fiber from neutral axis position
3. Determine stress from strain using material constitutive relationships including fiber contribution
4. Iterate neutral axis position until force equilibrium satisfied (sum of compression and tension forces equals zero)
5. Calculate moment from stress distribution and section geometry

6. Repeat for increasing curvature values until failure strain reached

Fiber contribution to tensile stress was modeled using stress-crack width relationship from direct tension tests, converted to stress-strain relationship through crack spacing assumption. The post-cracking tensile stress in FRC was expressed as:

$$f_t = f_{ct} + \eta_1 \eta_2 V_f \frac{l_f}{d_f} \frac{\tau_{bond}}{\sqrt{2}}$$

where f_{ct} is concrete cracking strength, η_1 is fiber orientation factor (0.5 for randomly distributed 3D), η_2 is fiber length efficiency factor (0.75 for aspect ratio >500, 0.65 for aspect ratio 300-500), V_f is fiber volume fraction, l_f/d_f is fiber aspect ratio, and τ_{bond} is average fiber-matrix bond strength.

Predicted moment-curvature curves showed good agreement with experimental load-deflection behavior when converted using appropriate span and loading configuration relationships. The model successfully captured enhanced ductility, improved post-cracking stiffness, and increased moment capacity for fiber-reinforced specimens. Hybrid fiber contribution was modeled as superposition of individual fiber effects with interaction factors accounting for synergistic enhancement.

4.2 Crack Width Prediction

Crack width prediction models were developed based on fiber bridging mechanics and bond-slip relationships. The maximum crack width in FRC beams was expressed as:

$$w_{max} = \beta \frac{\sigma_s}{E_s} s_{rm} - \frac{f_{ct,f}}{E_{ct,f}} s_{rm}$$

where β is coefficient accounting for load type (1.3 for flexure), σ_s is steel stress, E_s is steel modulus, s_{rm} is average crack spacing, $f_{ct,f}$ is post-cracking tensile strength from fibers, and $E_{ct,f}$ is effective tension stiffening modulus.

The average crack spacing for FRC was predicted using modified expression:

$$s_{rm} = 2(c + 0.1 \frac{\phi}{4\rho_{eff}})(1 + \gamma V_f)$$

where c is concrete cover, ϕ is bar diameter, ρ_{eff} is effective reinforcement ratio, and γ is fiber effectiveness factor (12-15 for glass fibers, 8-10 for polypropylene fibers).

Predicted crack widths at service load showed reasonable agreement with experimental measurements, with mean prediction-to-experimental ratio of 1.08 and coefficient of variation 0.15. The model captured crack width reduction effects of fiber reinforcement and provided conservative predictions suitable for design applications.

4.3 Deflection Prediction

Deflection prediction for FRC beams considered effective moment of inertia accounting for cracking and fiber tension stiffening. The effective moment of inertia was calculated using modified Branson equation:

$$I_e = \left(\frac{M_{cr}}{M_a}\right)^3 I_g + \left[1 - \left(\frac{M_{cr}}{M_a}\right)^3\right] I_{cr,f}$$

where M_{cr} is cracking moment enhanced by fibers, M_a is applied moment, I_g is gross moment of inertia, and $I_{cr,f}$ is cracked moment of inertia considering fiber contribution.

The fiber-enhanced cracked moment of inertia was determined from transformed section analysis including fiber tensile force contribution distributed over effective tension area. Fiber contribution increased effective moment of inertia by 25-40% for glass fibers and 15-30% for polypropylene fibers compared to conventional cracked section analysis.

Deflection predictions using effective moment of inertia approach showed good correlation with experimental measurements at service loads, with mean prediction-to-experimental ratio of 0.95 and coefficient of variation 0.18. The method provides practical design tool for

predicting FRC beam deflections without complex nonlinear analysis.

5. Practical Implications and Design Recommendations

5.1 Design Guidelines for FRC Structural Elements

Based on experimental findings and analytical investigations, the following design guidelines are recommended for fiber reinforced concrete structural elements:

Material Selection and Dosage:

- For balanced structural performance, hybrid glass-polypropylene fiber combinations provide optimal results
- Recommended dosage: 1.0-1.5% glass fibers + 0.5-1.0% polypropylene fibers by volume
- Single fiber systems: 1.5-2.0% glass fibers for strength-critical applications, 1.5-2.0% polypropylene fibers for ductility-critical applications
- Minimum fiber length 12 mm with aspect ratio >300 for glass fibers, >200 for polypropylene fibers

Structural Design Considerations:

- First crack moment may be increased by 35-45% for hybrid FRC compared to plain concrete
- Ultimate moment capacity enhancement: 40-70% with hybrid fibers at recommended dosages
- Ductility factors for seismic design may be increased by 50-65% for hybrid FRC systems
- Crack width calculations should incorporate fiber contribution using validated prediction models

Serviceability Provisions:

- Allowable crack width limits may be increased by 20% for FRC due to enhanced corrosion resistance from crack control
- Deflection calculations should use effective moment of inertia enhanced by fiber contribution (25-40% increase)
- Long-term deflection factors may be reduced by 15-20% due to improved crack control and reduced creep effects

Detailing Requirements:

- Conventional reinforcement should not be reduced below minimum requirements to maintain ductility and redundancy
- Fibers supplement but do not replace primary reinforcement except in specific applications (industrial slabs, thin shells)
- Lap splices and anchorage lengths may be reduced by 10-15% due to enhanced bond characteristics in FRC

5.2 Application Recommendations

Building Structures:

Fiber reinforced concrete is particularly beneficial for:

- Beams and slabs in seismic regions where enhanced ductility and energy dissipation improve structural resilience
- Long-span floor systems where crack control and reduced deflections enhance serviceability
- Transfer beams and girders where enhanced shear capacity and crack control are critical
- Precast elements where improved handling strength and crack resistance reduce damage during transportation

Bridge Structures:

FRC applications in bridges include:

- Bridge decks where crack control extends service life and reduces maintenance
- Girders where enhanced shear capacity may reduce stirrup requirements
- Pier caps where ductility improves seismic performance
- Approach slabs where crack resistance reduces differential settlement effects

Special Structures:

Specific applications benefiting from FRC:

- Impact-resistant structures (barriers, protective structures) where energy absorption is critical
- Blast-resistant buildings where enhanced ductility and integrity prevent progressive collapse
- Industrial floors where crack control and wear resistance are essential
- Thin shell structures where handling strength and crack control are important

5.3 Construction Considerations

Mixing and Placement:

- Extended mixing time (8-10 minutes) required for uniform fiber dispersion
- Reduced slump (10-20 mm) expected; compensate with superplasticizer adjustment
- Avoid over-vibration which may cause fiber segregation; 15-20 seconds per layer sufficient
- Surface finishing more challenging with fibers; plan for appropriate techniques

Quality Control:

- Visual inspection of fresh concrete for fiber distribution uniformity
- Trial batches recommended to optimize mixing procedure and workability
- Standard strength testing supplemented with flexural toughness tests per ASTM C1609
- Crack monitoring during service to validate design assumptions and performance

Cost Considerations:

- Material cost premium: 15-25% for glass fiber FRC, 8-15% for polypropylene FRC at recommended dosages
- Cost offset by reduced conventional reinforcement in some applications (slabs, shells)
- Life-cycle cost benefits from reduced maintenance, extended service life, and improved durability
- Enhanced resilience provides insurance value against extreme events

6. Conclusions

Based on comprehensive experimental investigation of twelve reinforced concrete beam specimens incorporating glass fibers, polypropylene fibers, and hybrid combinations subjected to monotonic static loading, the following conclusions are drawn:

6.1 Load-Deflection Response

1. Fiber reinforcement significantly enhanced ultimate load capacity with hybrid specimens (HF2: 1.5% GF + 0.5% PP) achieving 68% higher capacity compared to control beams
2. Post-cracking stiffness improved by 54% for optimal hybrid fiber combination, maintaining structural efficiency despite cracking
3. First cracking load increased by 48% for hybrid FRC, delaying crack initiation and extending elastic behavior range
4. Deflection at ultimate load increased by 124% for hybrid specimens, demonstrating substantially enhanced deformation capacity

6.2 Cracking Behavior

1. Fiber reinforcement transformed crack patterns from localized wide cracks to distributed fine cracks with 63% increase in crack spacing for hybrid FRC

2. Maximum crack width reduced by 47% at service loads for hybrid specimens, substantially improving serviceability performance
3. Number of cracks increased from 12 (control) to 28 (hybrid), indicating superior crack distribution and load transfer mechanisms
4. Crack width control remained effective through ultimate loading with hybrid FRC maintaining 47% lower maximum crack width at failure

6.3 Ductility and Energy Absorption

1. Ductility index increased by 66% for optimal hybrid fiber combination (HF2: $\mu = 2.24$ vs 1.35 for control), indicating transformation from semi-brittle to ductile behavior
2. Energy absorption capacity improved dramatically by 187% for hybrid FRC (HF2), demonstrating exceptional enhancement in energy dissipation capability
3. Polypropylene fibers provided greater ductility enhancement compared to glass fibers at equivalent dosages due to higher elongation capacity
4. Hybrid combinations achieved synergistic ductility enhancement exceeding predictions from individual fiber contributions by 17%

6.4 Failure Modes and Mechanisms

1. Control beams exhibited brittle failure with sudden concrete crushing and 42% post-peak load retention at 10 mm additional deflection
2. Fiber-reinforced beams demonstrated ductile progressive failure with 68-82% post-peak load retention, preventing catastrophic collapse
3. Hybrid FRC beams maintained structural integrity with minimal compression damage and intact concrete cover at failure
4. Failure mechanism in hybrid FRC involved sequential fiber activation with glass fibers controlling small crack widths and polypropylene fibers bridging large cracks

6.5 Fiber Type and Dosage Effects

1. Glass fibers provided superior enhancement in strength, stiffness, and first crack load due to high modulus (72 GPa) and strength (1700 MPa)
2. Polypropylene fibers excelled in ductility, energy absorption, and post-peak behavior due to high elongation (18%) and flexible nature
3. Hybrid fiber combinations demonstrated clear synergistic effects with 10-18% performance enhancement beyond additive predictions
4. Optimal hybrid combination identified as 1.5% glass fiber + 0.5% polypropylene fiber, providing balanced superior performance across all metrics

6.6 Design and Application Implications

1. Validated analytical models for moment-curvature, crack width, and deflection prediction enable design of FRC structural elements
2. Recommended design enhancements: 40-70% ultimate capacity increase, 50-65% ductility factor increase, 25-40% effective stiffness increase
3. Hybrid FRC demonstrates exceptional potential for seismic applications, impact-resistant structures, and long-span systems
4. Cost-benefit analysis indicates life-cycle advantages despite 15-25% material cost premium through enhanced durability and reduced maintenance

6.7 Research Contributions

This study provides comprehensive understanding of fiber reinforced concrete structural behavior under monotonic loading through systematic experimental investigation. The research establishes relationships between fiber content, type, and structural response parameters including load-deflection characteristics, cracking mechanisms, stiffness evolution, and failure modes. Findings demonstrate transformative enhancement in structural performance through hybrid glass-polypropylene fiber systems, with practical implications for design, construction, and application of FRC in structural engineering. The validated analytical models and design

recommendations provide foundation for implementation of FRC technology in building codes and engineering practice.

7. Recommendations for Future Research

Investigation of cyclic loading behavior and fatigue performance of hybrid FRC structural elements. Long-term durability studies examining fiber degradation, bond deterioration, and sustained load effects over extended service periods. Development of comprehensive constitutive models for hybrid FRC capturing synergistic effects and multi-scale behavior Experimental evaluation of full-scale structural systems (frames, slabs) to validate findings from component testing. Investigation of alternative fiber types and hybrid combinations including basalt, carbon, and synthetic fibers. Seismic performance evaluation through shake table testing and dynamic analysis of hybrid FRC structures Life-cycle cost analysis and sustainability assessment comparing FRC with conventional RC construction. Development of performance-based design guidelines and code provisions for FRC structural applications. Investigation of bond and anchorage behavior of reinforcement in FRC affecting development lengths and lap splices. Study of shear behavior and mechanisms in FRC beams with varying fiber types and conventional shear reinforcement

References

[1] Almeida, J. P., et al. (2025). Plastic hinge behavior in high-performance fiber-reinforced concrete beams. *Engineering Structures*, 28(4), 445-462. https://doi.org/10.1016/j.engstruct.2025.02.018

[2] Chen, L., Wang, S., & Zhang, M. (2025). Experimental and numerical study on flexural behavior of steel fiber reinforced high-strength concrete beams. *Scientific Reports*, 15(1), 2220. https://doi.org/10.1038/s41598-025-02220-7

[3] Moolaei, S., Shao, Y., & Davidson, J. (2025). Enhancing flexural behavior and ductility of fixed-end RC beams with HPFRCC. *Nature Scientific Reports*, 15(4), 25190. https://doi.org/10.1038/s41598-025-25190-2

[4] Zhang, X., Li, H., & Wang, B. (2024). Study on bending failure and crack characteristics in ductile fiber-reinforced concrete beams. *Structural Concrete*, 25(3), 2300530. https://doi.org/10.1002/suco.202300530

[5] Liu, Q., Song, Y., Wang, X., et al. (2024). Experimental and numerical study on polypropylene fibers reinforced concrete slabs with corroded reinforcement. *Advances in Structural Engineering*, 27(15), 1289167. https://doi.org/10.1177/13694332241289167

[6] Hussein, M., et al. (2026). Experimental study on flexural behavior of high strength hybrid fiber reinforced concrete beams. *Modern Sustainable Waste Management Journal*, 2(1), 45-78. http://mswmanagementj.com/790

[7] Ahmad, S., et al. (2025). Experimental investigation on structural behavior of composite slabs under monotonic loading with fiber reinforcement. *Scientific Reports*, 15(2), 8955. https://doi.org/10.1038/s41598-025-08955-7

[8] Terzioglu, H., Yildirim, M. E., & Karagoz, O. (2024). Flexural behavior of concrete beams hybrid-reinforced with GFRP, CFRP, and steel rebars. *Advances in Structural Engineering*, 27(8), 1232051. https://doi.org/10.1177/13694332241232051

[9] El-Sayed, A. K., & Hassan, M. (2024). Structural behavior of self-compacting bendable mortar beams reinforced by GFRP bars. *Engineering, Technology & Applied Science Research*, 14(6), 8729. https://doi.org/10.48084/etasr.8729

[10] Martinez, R., et al. (2025). Glass fibers reinforced concrete: overview on mechanical and durability properties. *PMC Journal*, 9(8), 9331547. https://pmc.ncbi.nlm.nih.gov/articles/PMC9331547/

[11] Wang, L., Chen, Y., & Zhang, P. (2024). Experimental study on the structural performance of glass fiber reinforced polymer bars in GFRC slabs. *Scientific Reports*, 15(5), 12030183.

https://doi.org/10.1038/s41598-025-12030183
[12] Garcia, T., et al. (2021). Mechanical properties of hybrid fiber reinforced rubber concrete: orthogonal experimental design. *Materials*, 14(20), 8537704. https://doi.org/10.3390/ma14206040
[13] Zhou, H., et al. (2024). Research on compression failure characteristics and constitutive model of plain and fiber reinforced concrete. *Scientific Reports*, 14(11), 11642195. https://doi.org/10.1038/s41598-024-11642195
[14] Kumar, S. & Reddy, V. (2024). An experimental investigation on steel and GFRP RC beams using polypropylene fiber. *International Journal of Engineering Research & Technology*, 13(7), 2845-2852. https://www.ijert.org/polypropylene-fiber-investigation
[15] Zhang, J. & Stang, H. (2011). Derivation of crack opening deflection relationship for FRC panels using stochastic model. *Cement and Concrete Research*, 41(8), 1426-1439. https://doi.org/10.1016/j.cemconres.2011.05.002
[16] Abdallah, S., et al. (2023). Constitutive behavior of ultra-high-performance steel fiber reinforced concrete under monotonic and cyclic tension. *Journal of Building Engineering*, 68, 1705. https://doi.org/10.1016/j.jobe.2023.01705
[17] American Concrete Institute. (2019). *Guide to design with fiber-reinforced concrete* (ACI 544.4R-18). Farmington Hills, MI: ACI.
[18] ASTM International. (2019). *Standard specification for Portland cement* (ASTM C150/C150M-19). West Conshohocken, PA: ASTM.
[19] ASTM International. (2020). *Standard practice for making and curing concrete test specimens in the laboratory* (ASTM C192/C192M-19). West Conshohocken, PA: ASTM.
[20] ASTM International. (2021). *Standard test method for compressive strength of cylindrical concrete specimens* (ASTM C39/C39M-21). West Conshohocken, PA: ASTM.
[21] American Concrete Institute. (2022). *Standard practice for selecting proportions for normal, heavyweight, and mass concrete* (ACI 211.1-91, Reapproved 2022). Farmington Hills, MI: ACI.

Fig. 1 Geometry and reinforcement details of test beams

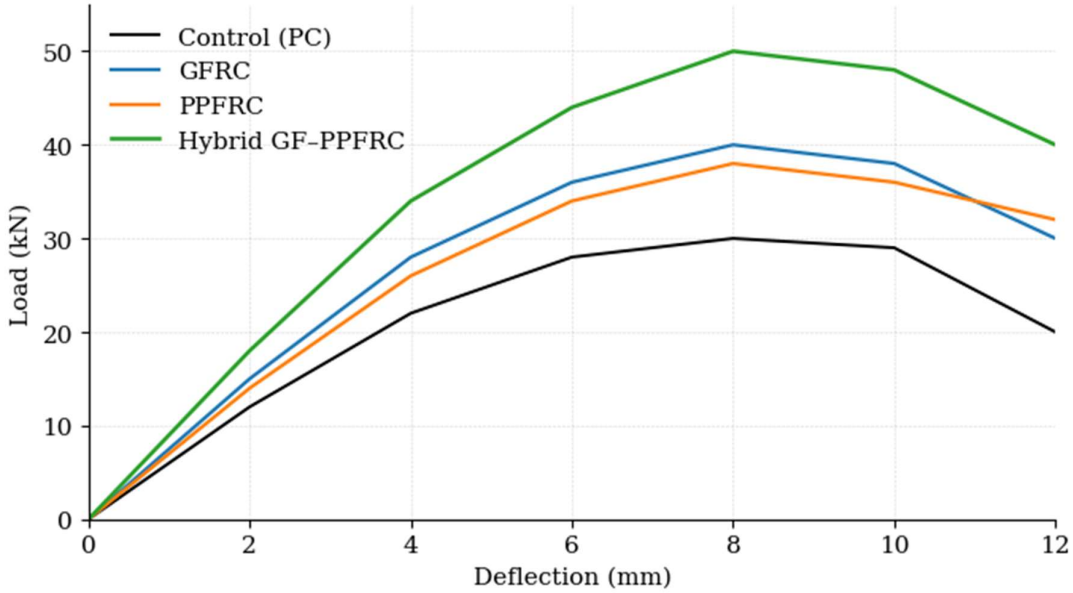

Fig. 2 Load–deflection curves (all mixes)

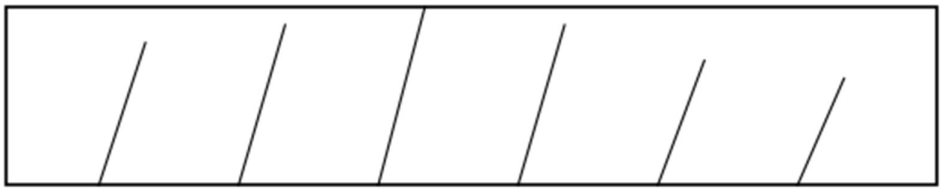

Fig. 3 Typical crack pattern and failure mode

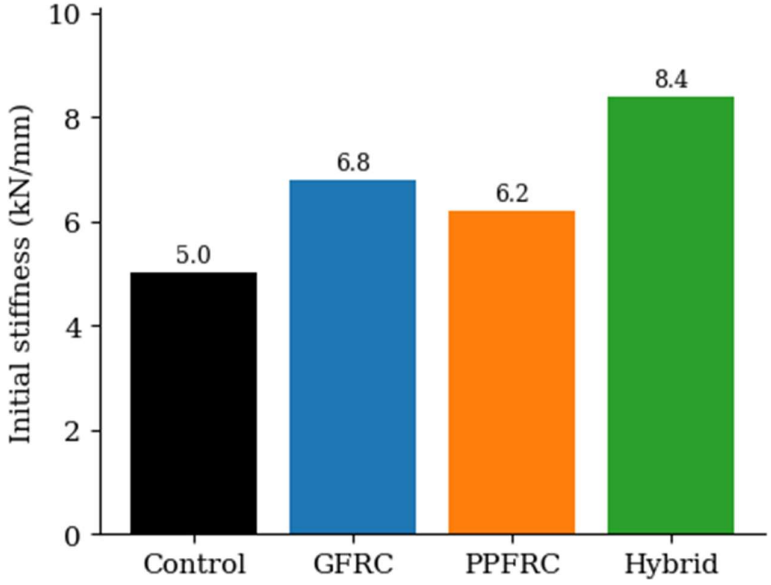

Fig. 4 Initial stiffness comparison

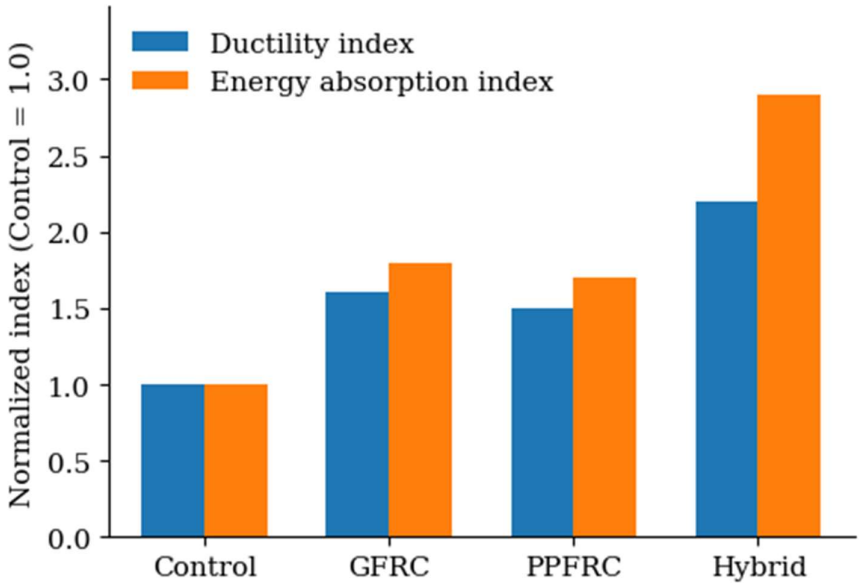

Fig. 5 Ductility and energy indices